Diagnosis of Sensor Faults in PMSM and Drive System Based on Structural Analysis

Saeed Hasan Ebrahimi, Martin Choux, and Van Khang Huynh

Department of Engineering Sciences
University of Agder
NO-4879 Grimstad, Norway

Abstract – This paper presents a model-based fault diagnosis method to detect sensor faults in permanent magnet synchronous motor (PMSM) drives based on structural analysis technique. The structural model is built based on the dynamic model of the PMSM in matrix form, including unknown variables, known variables, and faults. The Dulmage–Mendelsohn (DM) decomposition is applied to evaluate the redundancy of the model and obtain redundant testable sub-models. These testable redundant sub-models are used to form residuals to observe the system state, and distinguish between healthy and faulty conditions.This work investigates faults in eleven sensors in a PMSM drive, thus nine structured residuals are designed to detect and isolate the investigated faults, which are applied to the system at different time intervals. Finally, the effectiveness of the proposed diagnostic approach is experimentally validated on an in-house setup of inverter-fed PMSMs.

D.1 Introduction

Permanent Magnet Synchronous Motors (PMSMs) are widely used in many high-performance drive applications including robotic systems, transportation, and offshore industries. Their key features of higher efficiency, power density, and controlability make them more attractive than other motors [1, 2]. Since controlling PMSM drives must rely on different sensors to achieve their goals and ensure full functionality of the overall system, condition monitoring of these sensors is necessary to guarantee the high reliability [3, 4].

Extensive research work has been conducted in diagnosis of sensor faults in an electric drive system [5–7]. Most of these techniques are observer-based to investigate faults in different combinations of sensors involved in the system by comparing the measured signals with corresponding estimated ones. For instance, observer-based speed and load torque sensor faults have been investigated in [6], while an adaptive observer has been employed to detect speed, dc bus voltage, and current faults by estimating sensor signals values [7]. Although these proposed observers have been proven to be effective in early detection of sensor faults, isolating faults may become quite challenging, especially when multiple sensors are involved in the system. Thus, structural analysis was proposed as an alternative model-based approach for detecting and isolating multiple faults in a complex system [8]. The theoretical basis of structural analysis technique has been studied and well developed in the literature [9–11]. So far, structural analysis are implemented on different systems including automotive engine [12], hybrid vehicle [13], and electric drive

system with eight sensors [8], but the existing works only focus on limited fault types and vehicles alone. It is important to extend this approach to deal with faults in PMSM drives in hash environments, like offshore industry, where the fault context might not only have higher number of sensor faults, but also higher fault diversity, i.e, dc capacitors, or dc link.

This paper presents a model-based fault detection and isolation methodology based on structural analysis for investigating eleven sensor faults in PMSMs, being applied to a more generalized electric drive system and motor's structure where many different sensors are required for condition-monitoring of the system. The required measurements include three-phase voltage and current sensors, DC bus voltage and current sensors, motor's angular velocity and position, and load torque. To build a structure model, a combination of healthy dynamic mathematical models of PMSM both in *abc* and *dq* frames including all the aforementioned sensors is employed, and specific terms related to each fault are added to the corresponding equations. These added terms include the deviations in the measured signals of each sensor caused by dc offsets, gain change, amplitude imbalance, and generally any sort of mismeasurement appearing in the corresponding equations. Furthermore, the analytical redundancy of the model is determined based on the motor and drive system's structural model. This redundant model is then subdivided into smaller over-determined testable subsystems, in which the faults are detected, and isolated. The novelty of this study is that not only more sensors are considered and therefore, more measurements, equations, and redundancy are added to the system but also, the effect of dc bus voltage and current as well as load torque sensors is taken into consideration, making the diagnostic system more effective to detect any faults. To observe the presence of faults, nine sequential residuals are designed and implemented from which certain combination of these residuals can be employed to isolate each fault. Finally, the effectiveness of the proposed model is validated on a experimental setup of inverter-fed PM synchronous motors.

D.2 Structural Analysis for PMSM and Drive System

Structural analysis is a mathematical algorithm that extracts the analytic redundant relations (ARRs) of a system based on the mathematical equations describing its dynamic [11, 14]. This structural model is initiated by an incidence matrix in which each row connects an equation to the corresponding unknown variables, known variables, and faults. Next, the rows and columns are rearranged in a way to form a diagonal structure - called Dulmage–Mendelsohn (DM) decomposition - to obtain the analytic redundancy of the system. After finding the exact determined part of the system, in which the number of equations is equal to the number of variables, the other part of the system is an analytic redundant part. This redundant part is used to identify several smaller over-constrained subsystems, being called set of ARRs. Depending on the fault signature of this set of ARRs, each considered fault might be detected or even isolated. Subsequently, several diagnostic tests are designed to inform the presence of each fault. This study

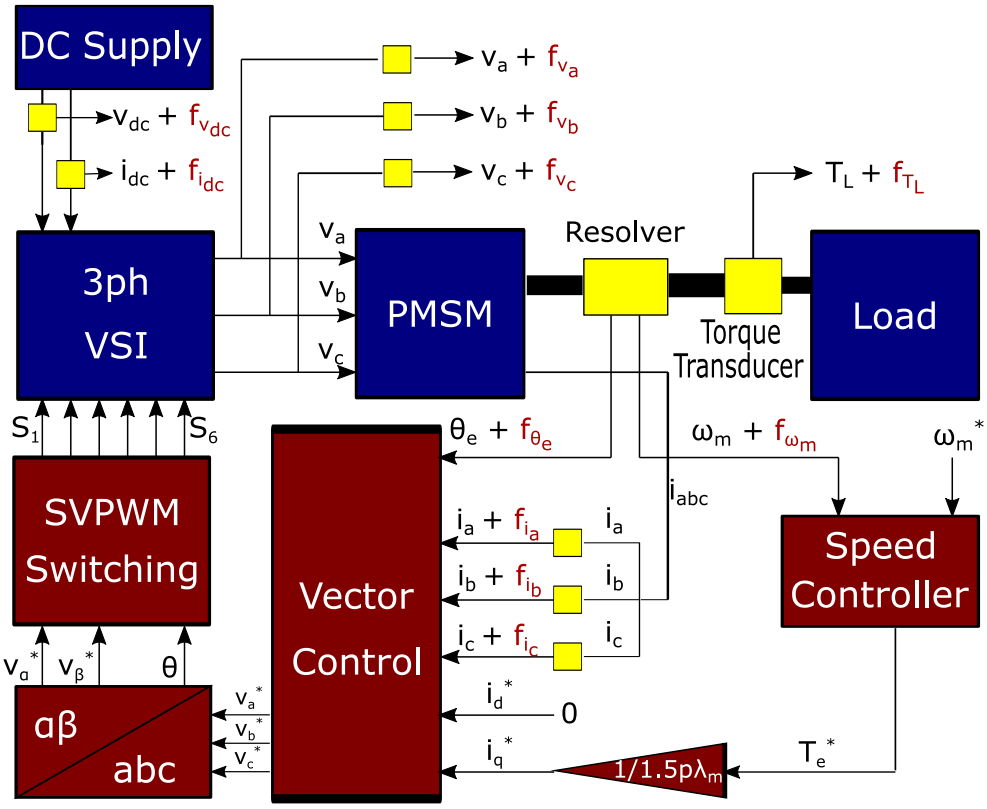

Figure D.1: Modeling diagram of PMSM and drive system.

presents a structural analysis of a PMSM and drive system containing sensor faults, and diagnostic tests are proposed for sensor detection and isolation. Fig. D.1 shows the modeling diagram of the PMSM and drive system components containing sensor faults, whereas the parameters are defined in the following section.

D.2.1 Mathematical Model of PMSM Drive

The mathematical model of a PMSM and drive system with sensor faults is described by equations $e_1 - e_{11}$ as shown in Eq. (D.1), where v_a, v_b, and v_c are the stator three phase voltages. Inside the PMSM block, v_d and v_q are the obtained using $e_1 - e_2$. Through $e_3 - e_4$, i_d and i_q are obtained which are needed for electromagnetic torque T_e calculation in e_9 and consequently, angular speed ω_m calculation in e_{10}. Feedback currents, i_a, i_b, and i_c, are obtained through $e_5 - e_7$. In addition, λ_m is the flux produced by PMs; R_s is the stator phase resistance; L_d and L_q are the dq inductances; v_{dc} and i_{dc} are the dc bus voltage and current; η_{inv} is the inverter's efficiency; T_L is the load torque; θ_e is the electric angular position; p is the number of pole pairs; J is the rotor inertia, and b is the

viscous damping coefficient.

$$
\begin{aligned}
e_1 :& v_d = \frac{2}{3}[v_a \cos\theta_e + v_b \cos(\theta_e - 2\pi/3) \\
& + v_c \cos(\theta_e + 2\pi/3)] \\
e_2 :& v_q = -\frac{2}{3}[v_a \sin\theta_e + v_b \sin(\theta_e - 2\pi/3) \\
& + v_c \sin(\theta_e + 2\pi/3)] \\
e_3 :& \frac{di_d}{dt} = \frac{1}{L_d}[v_d - R_s i_d + p\omega_m L_q i_q] \\
e_4 :& \frac{di_q}{dt} = \frac{1}{L_q}[v_q - R_s i_q - p\omega_m L_d i_d - p\omega_m \lambda_m] \\
e_5 :& i_a = i_d \cos\theta_e - i_q \sin\theta_e \\
e_6 :& i_b = i_d \cos(\theta_e - 2\pi/3) - i_q \sin(\theta_e - 2\pi/3) \\
e_7 :& i_c = i_d \cos(\theta_e + 2\pi/3) - i_q \sin(\theta_e + 2\pi/3) \\
e_8 :& v_{dc} i_{dc} \eta_{inv} = v_a i_a + v_b i_b + v_c i_c \\
e_9 :& T_e = \frac{3}{2} p[(L_d - L_q) i_d + \lambda_m] i_q \\
e_{10} :& \frac{d\omega_m}{dt} = \frac{1}{J}(T_e - b\omega_m - T_L) \\
e_{11} :& \frac{d\theta_e}{dt} = p\omega_m
\end{aligned}
\tag{D.1}
$$

The known variables y in the structural model include three-phase voltages (y_{v_a}, y_{v_b}, y_{v_c}), three-phase currents (y_{i_a}, y_{i_b}, y_{i_c}), dc bus voltage and current ($y_{v_{dc}}$, $y_{i_{dc}}$), electric angular position (y_{θ_e}), angular speed (y_{ω_m}), and load torque (y_{T_L}). Since these known variables come from sensor measurements, corresponding fault terms f are added to the equations, i.e., y_{v_a}, y_{v_b}, y_{v_c}, y_{i_a}, y_{i_b}, y_{i_c}, $y_{v_{dc}}$, $y_{i_{dc}}$, y_{θ_e}, y_{ω_m}, and y_{T_L}, resulting in 11 measurements and faults in total (shown in Eq. (D.2).).

$$
\begin{aligned}
m_1 &: y_{v_a} = v_a + f_{v_a} & m_7 &: y_{v_{dc}} = v_{dc} + f_{v_{dc}} \\
m_2 &: y_{v_b} = v_b + f_{v_b} & m_8 &: y_{i_{dc}} = i_{dc} + f_{i_{dc}} \\
m_3 &: y_{v_c} = v_c + f_{v_c} & m_9 &: y_{\theta_e} = \theta_e + f_{\theta_e} \\
m_4 &: y_{i_a} = i_a + f_{i_a} & m_{10} &: y_{\omega_m} = \omega_m + f_{\omega_m} \\
m_5 &: y_{i_b} = i_b + f_{i_b} & m_{11} &: y_{T_L} = T_L + f_{T_L} \\
m_6 &: y_{i_c} = i_c + f_{i_c}
\end{aligned}
\tag{D.2}
$$

In addition, the mathematical model of PMSM includes 4 differential constraints of unknown variables, which are shown in Eq. (D.3).

$$
\begin{aligned}
d_1 &: \tfrac{di_d}{dt} = \tfrac{d}{dt}(i_d) & d_2 &: \tfrac{di_q}{dt} = \tfrac{d}{dt}(i_q) \\
d_3 &: \tfrac{d\theta_e}{dt} = \tfrac{d}{dt}(\theta_e) & d_4 &: \tfrac{d\omega_m}{dt} = \tfrac{d}{dt}(\omega_m)
\end{aligned}
\tag{D.3}
$$

D.2.2 Structural Model and Analytical Redundancy of the PMSM

The structural model of PMSM drive with sensor faults is obtained based on the defined mathematical model in Eqs. (D.1)-(D.3), as shown in Fig. D.2. The incidence matrix

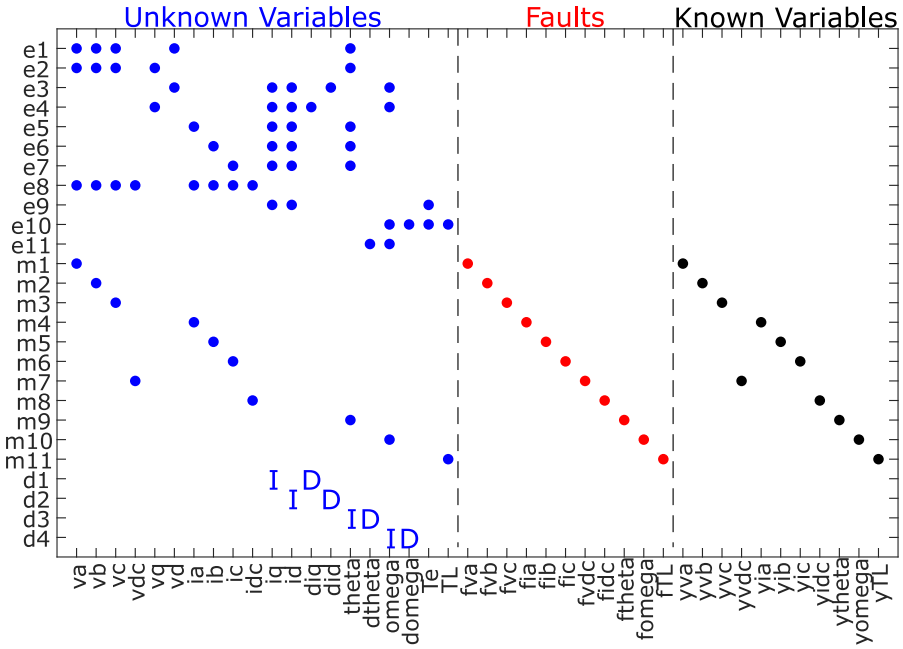

Figure D.2: PMSM drive structural model.

contains 26 rows, representing the 11 defined equations in Eq. (D.1), 11 measured known variables in Eq. (D.2), and the 4 differential constraints of unknown variables as shown in Eq. (D.3). The columns of the incidence matrix are subdivided into three groups of unknown variables, known variables, and faults, and each equation is connected to its relevant constraint in any of the three groups through each row. As shown in Fig. D.2, the differentiated and integrated variable relations are indicated by "D" and "I" signs, respectively.

For a fault to be detectable and then isolable , it should lie in the structurally over-determined part of the structural model, where there are more equations than unknown variables [10]. To accomplish this, DM decomposition tool is employed to evaluate the redundancy of the model. This is done by restructuring the structural model into an upper triangle shape by rearranging the rows and the columns of the incidence matrix. Fig. D.3 shows the DM decomposition for PMSM and drive system structural model, where the analytic redundant part of the system is expressed containing all the faults.

D.3 Diagnostic Test Design

This section presents the procedure of designing diagnostic tests for sensor faults in PMSM and drive system. First, the analytic redundant part is divided into smaller redundant subsystems, and then sequential residuals are derived to detect each fault.

D.3.1 Finding Testable Sub-Models

The analytic redundant part of the system is subdivided into efficient redundant testable sub-models, called Minimal Structurally Over-determined (MSO) sets, as proposed in [9]. The studied PMSM drive renders 20 unknown variables, 11 known variables, 11 fault

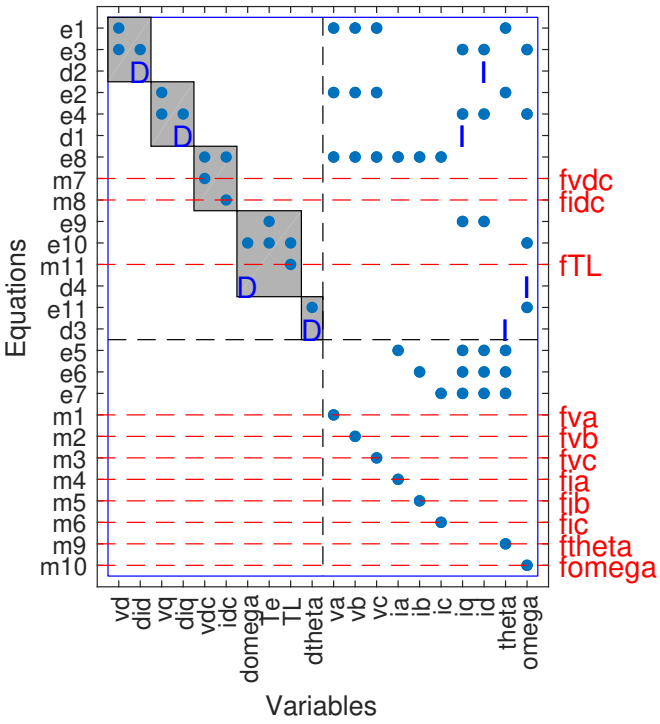

Figure D.3: DM decomposition for PMSM and drive system.

variables, and 26 equations including 4 differential constraints, resulting in the degree of redundancy 6 and 1525 MSO sets. Since the number of MSO sets increases exponentially in the degree of redundancy, Minimal Test Equation Support (MTES) sets is used instead, allowing for significantly reducing computational complexity without reducing the possible diagnosis performance [15]. The reason is that MTES sets are obtained in a way that the effect of faults is considered. In other terms, MTES sets are subsets of MSO sets, in which the effect of faults is visible. Here, the degree of redundancy for MTES sets is 1, and the algorithm yields 168 MTES sets. Next, different combinations of MTES sets are acquired, and the one that yields an acceptable value for diagnosability index (m_D) [16], is chosen to form residuals. Fig. D.4 shows the selected MTES sets found for the considered system, and the equations that are used in each MTES set for which diagnosability index, are obtained as $m_D = 4.45$. Fig. D.5 shows the signature matrix of MTES sets, indicating which faults appear in each MTES set. It is observed that the distance between any two faults ($D(V_{f_i}, V_{f_j})$) in this selection is more than 2, except $D(f_{v_{dc}}, f_{i_{dc}})$ are 0. This means that all the faults except $f_{v_{dc}}$ and $f_{i_{dc}}$ are isolable.

$MTES_1$ includes only f_{θ_e} and f_{ω_m} fault terms. It means that it can be used for either angular position or speed measurement faults. $MTES_3$ contains f_{i_b}, f_{i_c}, f_{θ_e}, and f_{T_L} fault terms, therefore, it can be used to detect load torque measurement fault. $MTES_{153}$ contain f_{v_a}, f_{v_b}, f_{v_c}, $f_{v_{dc}}$, $f_{i_{dc}}$, and f_{θ_e} fault terms, and by calculating the three-phase currents based on these measurements, $f_{v_{dc}}$ and $f_{i_{dc}}$ measurement faults can be detected. Each of the $MTES_{146}$, $MTES_{57}$, and $MTES_{112}$ sets contain two of the phase-voltages, two of the phase currents, and angular position, thus, they can be used in forming the residuals to detect f_{v_a}, f_{v_b}, and f_{v_c} measurement faults. Subsequently, each of the $MTES_{165}$, $MTES_{160}$, and $MTES_{156}$ sets contain the three-phase voltages, one of the phase currents,

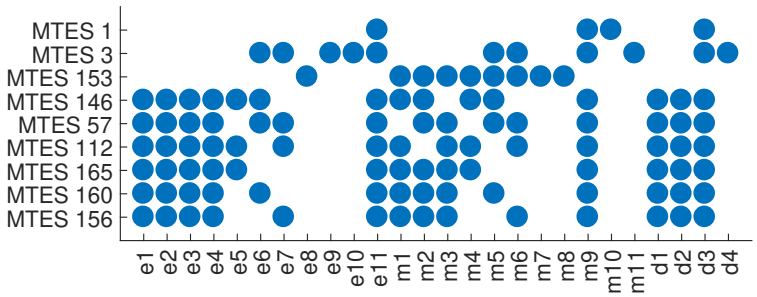

Figure D.4: MTES sets.

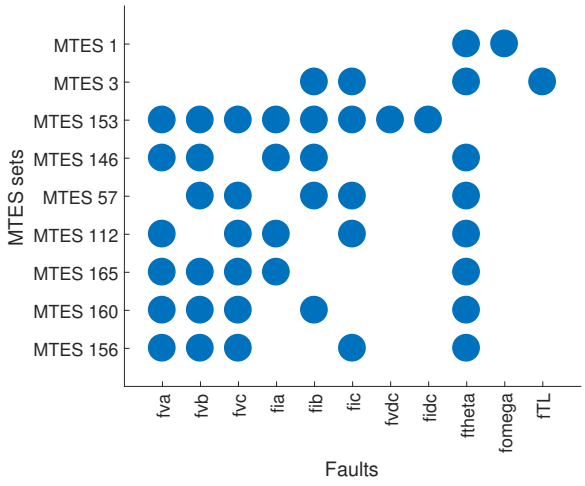

Figure D.5: Fault signature matrix of MTES sets.

and angular position, therefore, they can be used in forming the residuals to detect f_{i_a}, f_{i_b}, and f_{i_c} measurement faults.

D.3.2 Sequential Residuals for Detecting the Faults

In this section, 9 sequential residuals ($R_1 - R_9$) are derived based on the selected MTES sets. These residuals aim to detect all the considered faults and a combination of them can be used to isolate each fault.

1. R_1: $MTES_1$ is used for deriving R_1 based on m_9 in Eq. (D.2):

$$m_9 : R_1 = y_{\theta_e} - \theta_e \tag{D.4}$$

And the sequence of deriving θ_e is as follows:

$$\begin{aligned} SV &: \theta_e = \theta_{state} \\ m_{10} &: y_{\omega_m} = \omega_m \\ e_{11} &: \frac{d\theta_e}{dt} = p\omega_m \end{aligned} \tag{D.5}$$

Where θ_{state} is a state variables (SV) and will be updated after R_1 is calculated using integral form of d_3 in Eq. (D.3).

2. R_2: $MTES_3$ is used for deriving R_2 based on m_{11} in Eq. (D.2):

$$m_{11} : R_2 = y_{T_L} - T_L \tag{D.6}$$

To calculate T_L, e_9 and e_{10} must be used as shown in $MTES_3$ equation sets Fig. D.4. Knowing that θ_e is obtained directly from measurement, ω_m and $\frac{d\omega_m}{dt}$ can be easily calculated using the sequence of d_3, e_{11}, and d_4. Then i_b and i_c measurements are used to calculate i_d and i_q from e_6 and e_7 as follows:

$$\begin{aligned} i_d &= \frac{-2}{\sqrt{3}}[i_b \sin(\theta_e + \frac{2\pi}{3}) - i_c \sin(\theta_e - \frac{2\pi}{3})] \\ i_q &= \frac{-2}{\sqrt{3}}[i_b \cos(\theta_e + \frac{2\pi}{3}) - i_c \cos(\theta_e - \frac{2\pi}{3})] \end{aligned} \tag{D.7}$$

3. R_3: $MTES_{153}$ is used for deriving R_3 based on e_8 in Eq. (D.2):

$$e_8 : R_3 = v_{dc} i_{dc} \eta_{inv} - v_a i_a - v_b i_b - v_c i_c \tag{D.8}$$

where all the variables come from the measurements.

4. R_4: $MTES_{146}$ is used for deriving R_4 based on m_1 in Eq. (D.2):

$$m_1 : R_4 = y_{v_a} - v_a \tag{D.9}$$

To calculate v_a, θ_e is obtained directly from measurement, and ω_m is subsequently calculated using the sequence of d_3 and e_{11}. Similar to Eq. (D.7), two current measurements (i_a and i_b) are used to calculate i_d and i_q but this time from e_5 and e_6. Then $\frac{di_d}{dt}$ and $\frac{di_q}{dt}$ are obtained from d_1 and d_2 and used in e_3 and e_4 to form v_d and v_q. Finally, v_a is calculated from e_1 and e_2 as follows:

$$v_a = v_d \cos\theta_e - v_q \sin\theta_e \tag{D.10}$$

5. R_5 and R_6 follow similar procedure mentioned for R_4 to find the difference between measured and calculated phase b and phase c voltages based on $MTES_{57}$ and $MTES_{112}$, respectively.

6. R_7: $MTES_{165}$ is used for deriving R_7 based on based on m_4 in Eq. (D.2):

$$m_4 : R_7 = y_{i_a} - i_a \tag{D.11}$$

To calculate i_a, θ_e is obtained directly from measurement, and ω_m is subsequently calculated using the sequence of d_3 and e_{11}. Then the measured values of v_a, v_b, and v_c are used in e_1 and e_2 to get to v_d and v_q. Next, $\frac{di_d}{dt}$ and $\frac{di_q}{dt}$ are obtained from d_1 and d_2 and finally i_a is calculated from e_5 as follows:

$$i_a = i_d \cos\theta_e - i_q \sin\theta_e \tag{D.12}$$

7. R_8 and R_9 follow similar procedure mentioned for R_7 to find the difference between measured and calculated phase b and phase c currents based on $MTES_{160}$ and $MTES_{156}$, respectively.

D.4 Experiments and Results

The proposed diagnostic method is validated through experimental results in this section. Fig. D.6 shows the experimental setup, where two identical PMSMs are mechanically coupled to form a motor-generator set. A torque transducer is placed in between the motors to measure the load torque, which can be varied through resistive load of the generator. The motor is controlled by an inverter and the sensors are powered by a low voltage dc supply. Finally, a dSpace MicrolabBox is used to control the motor and collect the sensor data. The parameters of studied PMSMs are listed in Table D.1.

A ramp speed reference was applied on the motor to test the residual responses under nominal operating conditions of 1200 rpm. Fig. D.7 shows the speed reference and the motor's speed during the time of the operation.

After reaching the nominal speed, the measurement faults are applied at different time intervals. To cover all the possible measurement errors, different measurement errors have been applied including dc offset values for current sensors, speed and torque sensors, gain change for voltage sensors, and imbalance in angle measurement. At $t = 1 - 2s$, there appears a $+0.2rad/s$ offset in ω_m measurement; at $t = 3 - 4s$, there is a $+1N.m$ offset in T_L measurement; at $t = 5 - 6s$, the inverter has a $+2\%$ gain increase in v_{dc} measurement; at $t = 7 - 8s$, the inverter has a $+0.04A$ offset in i_{dc} measurement; at $t = 10 - 11s$, there appears a $+4\%$ gain change in v_a measurement;at $t = 12 - 13s$, there is a $+4\%$ gain change in v_b measurement;at $t = 14 - 15s$, appears a $+4\%$ gain change in v_c measurement;at $t = 17 - 18s$, there is a $+2A$ offset in i_a measurement;at $t = 19 - 20s$, there is a $+2A$ offset in i_b measurement;at $t = 21 - 22s$, there is a $+2A$ offset in i_b measurement; and finally at $t = 23 - 24s$, there is a $+0.01$ amplitude imbalance in θ_e measurement. Fig. D.8 shows the sequence of applied sensor faults.

The residual responses for the sensor faults are obtained after the motor reaches steady-state condition i.e. constant 1200 rpm of speed and 14 N.m of load torque ($t = 5 - 25s$

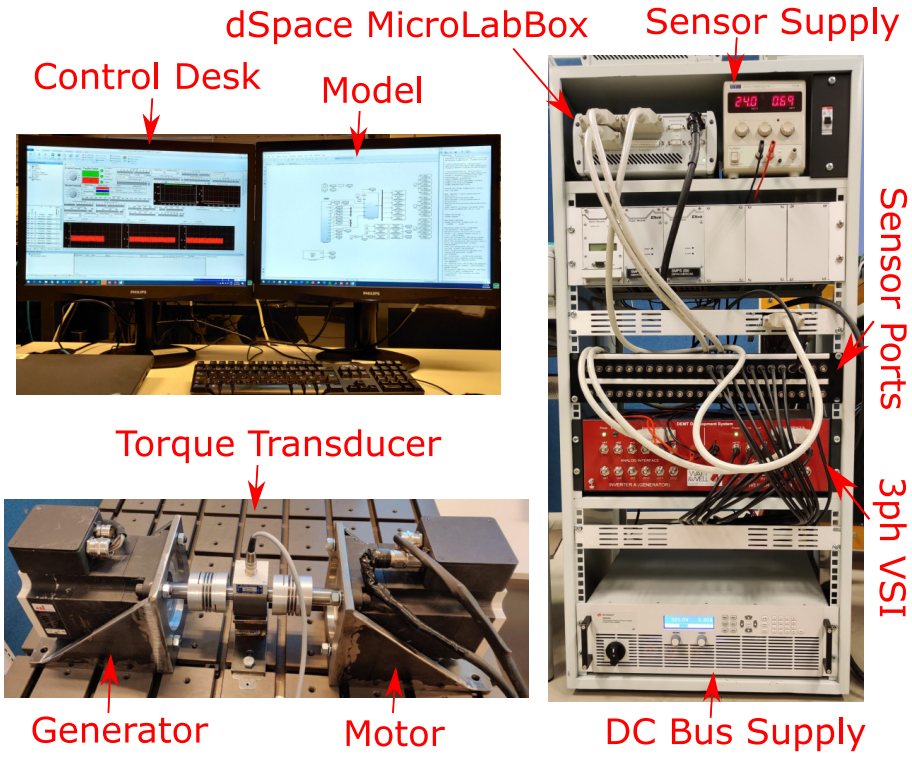

Figure D.6: Experimental setup.

Table D.1: Parameters of PM Synchronous Motor

Symbol	Parameter	Value	Unit
V_{dc}	Rated dc bus voltage	320	V
I_s	Rated rms phase current	5.9	A
T_{out}	Output Torque	14	$N.m$
n_s	Rated speed	1200	rpm
R_s	Phase resistance	1.125	Ω
L_q, L_d	Q and D axes inductances	8.75	mH
J	Rotor inertia	13.558	$kg.cm^2$
b	Rotor damping factor	0.00295	$N.m.s/rad$
λ_m	Flux linkage of PMs	0.1554	Web
p	Pole-pairs	4	

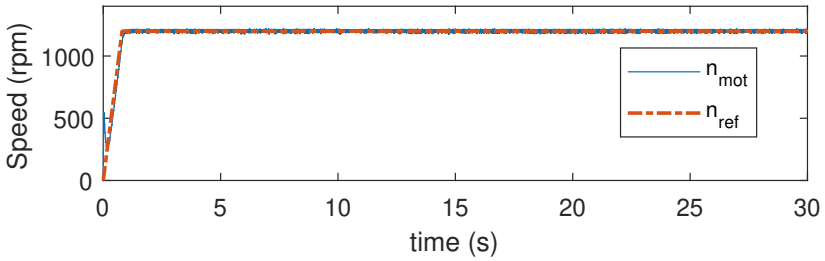

Figure D.7: Motor's speed and reference speed.

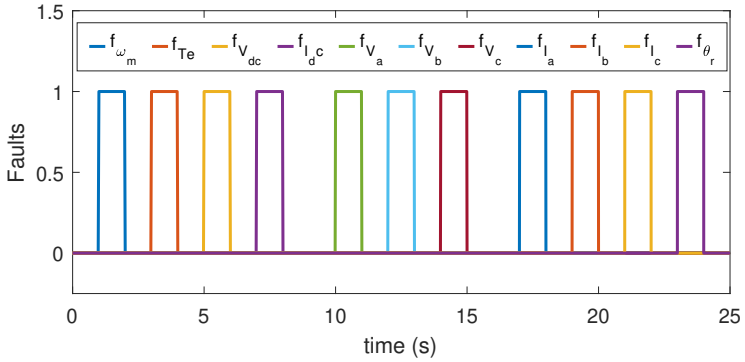

Figure D.8: Sequence of of faults.

in Fig. D.7). All the residual responses are filtered using a low-pass filter for better demonstration and shown in Fig. D.9. For $t = 0 - 1s$, the motor is operating in healthy mode and all the residuals remain averagely zero (neglecting the noise) since the signal values from the measurement and the calculations in each residual are similar. When the first fault i.e. f_{ω_m} occurs, only R_1 is affected and obtains a non-zero value. similarly when f_{T_L} occurs next, only R_2 is affected and obtains a non-zero value. The inverter faults $f_{v_{dc}}$ and $f_{i_{dc}}$ appear next and trigger R_3 at different time intervals. when the phase-a voltage fault f_{v_a} occurs at $t = 10 - 11s$, residuals [R_3, R_4, R_6, R_7, R_8, R_9] are triggered as expected in fault signature matrix (Fig. D.5). Similarly, f_{v_b} and f_{v_c} trigger residuals [R_3, R_4, R_5, R_7, R_8, R_9] and residuals [R_3, R_5, R_6, R_7, R_8, R_9], respectively. Next one is the phase-a current fault f_{i_a} which occurs at $t = 17 - 18s$ and residuals [R_3, R_4, R_6, R_7] are triggered. Similarly, f_{i_b} and f_{i_c} trigger residuals [R_2, R_3, R_4, R_5, R_8] and residuals [R_2, R_3, R_5, R_6, R_9], respectively.

As shown in Fig. D.9, all faults are detectable and each fault can trigger at least one of the designed residuals $R_1 - R_9$. The faults f_{ω_m}, f_{T_L}, $f_{v_{dc}}$, and $f_{i_{dc}}$ only trigger one residual during their presence and therefore, very easy to be isolated. The rest trigger multiple but unique combinations of residuals. Based on this, the behavior and response of specific combinations of residuals can be used as the ground for detection and isolation of these faults in the PMSM and drive system.

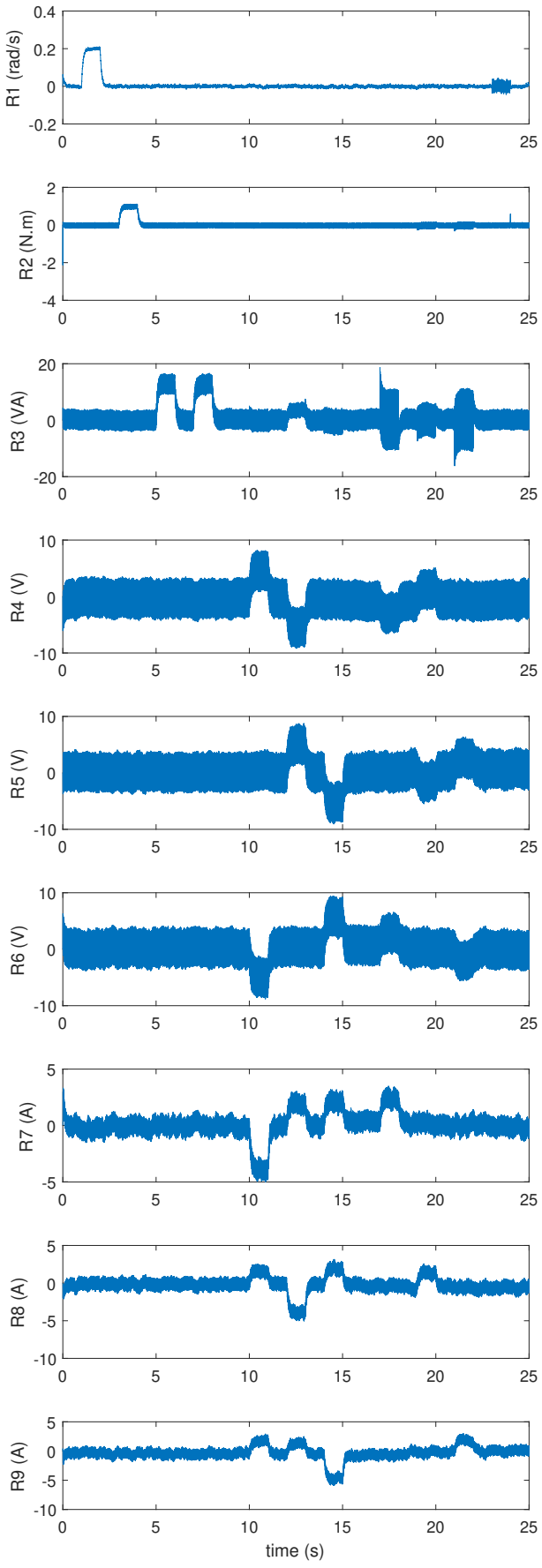

Figure D.9: Response of residuals.

D.5 Conclusion

This paper presents a method to detect and isolate sensor faults in a PMSM drive based on structural analysis. Not only are more sensor faults investigated compared to previous studies, but also the dc bus voltage and current are involved in the system. Structural analysis is employed to obtain the redundant part of the PMSM drive using DM decomposition. 9 sequential residuals are derived based on the fault terms that appear in each of the MTES sets to detect and isolate 11 faults in the sensors including voltage, current, load torque, speed, and angular position sensors. The proposed model is implemented experimentally and the behavior of residuals during mentioned faults are investigated in different time intervals. The experimental results show that residuals are able to efficiently detect and isolate faults in the laboratory test, proving the effectiveness of this diagnostic approach.

References

[1] Jun Hang, Han Wu, Jibo Zhang, Shichuan Ding, Yourui Huang, and Wei Hua. Cost function-based open-phase fault diagnosis for pmsm drive system with model predictive current control. *IEEE Transactions on Power Electronics*, 36(3):2574–2583, 2020.

[2] Xueqing Wang, Zheng Wang, Zhixian Xu, Jiangbiao He, and Wenxiang Zhao. Diagnosis and tolerance of common electrical faults in t-type three-level inverters fed dual three-phase pmsm drives. *IEEE Transactions on Power Electronics*, 35(2):1753–1769, 2019.

[3] Faa-Jeng Lin and Yueh-Shan Lin. A robust pm synchronous motor drive with adaptive uncertainty observer. *IEEE Transactions on Energy Conversion*, 14(4):989–995, 1999.

[4] Se-Kyo Chung, Hyun-Soo Kim, Chang-Gyun Kim, and Myung-Joong Youn. A new instantaneous torque control of pm synchronous motor for high-performance direct-drive applications. *IEEE Transactions on Power Electronics*, 13(3):388–400, 1998.

[5] F Grouz, L Sbita, and M Boussak. Current sensors gain faults detection and isolation based on an adaptive observer for pmsm drives. In *10th International Multi-Conferences on Systems, Signals & Devices 2013 (SSD13)*, pages 1–6. IEEE, 2013.

[6] Jaroslaw Guzinski, Haitham Abu-Rub, Marc Diguet, Zbigniew Krzeminski, and Arkadiusz Lewicki. Speed and load torque observer application in high-speed train electric drive. *IEEE Transactions on Industrial Electronics*, 57(2):565–574, 2009.

[7] Tooraj Abbasian Najafabadi, Farzad R Salmasi, and Parviz Jabehdar-Maralani. Detection and isolation of speed-, dc-link voltage-, and current-sensor faults based on an adaptive observer in induction-motor drives. *IEEE Transactions on Industrial Electronics*, 58(5):1662–1672, 2010.

[8] Jiyu Zhang, Hongyang Yao, and Giorgio Rizzoni. Fault diagnosis for electric drive systems of electrified vehicles based on structural analysis. *IEEE Transactions on Vehicular Technology*, 66(2):1027–1039, 2016.

[9] Mattias Krysander, Jan Åslund, and Mattias Nyberg. An efficient algorithm for finding minimal overconstrained subsystems for model-based diagnosis. *IEEE Transactions on Systems, Man, and Cybernetics-Part A: Systems and Humans*, 38(1):197–206, 2007.

[10] Mattias Krysander and Erik Frisk. Sensor placement for fault diagnosis. *IEEE Transactions on Systems, Man, and Cybernetics-Part A: Systems and Humans*, 38(6):1398–1410, 2008.

[11] Mogens Blanke, Michel Kinnaert, Jan Lunze, and Marcel Staroswiecki. Diagnosis and fault tolerant control, 2016.

[12] Carl Svärd, Mattias Nyberg, Erik Frisk, and Mattias Krysander. Automotive engine fdi by application of an automated model-based and data-driven design methodology. *Control Engineering Practice*, 21(4):455–472, 2013.

[13] Christofer Sundström, Erik Frisk, and Lars Nielsen. Selecting and utilizing sequential residual generators in fdi applied to hybrid vehicles. *IEEE Transactions on Systems, Man, and Cybernetics: Systems*, 44(2):172–185, 2013.

[14] Mattias Krysander. *Design and analysis of diagnosis systems using structural methods*. PhD thesis, PhD thesis, Linköping Univ., Linköping, Sweden, 2006.

[15] Mattias Krysander, Jan Åslund, and Erik Frisk. A structural algorithm for finding testable sub-models and multiple fault isolability analysis. In *21st International Workshop on Principles of Diagnosis (DX-10), Portland, Oregon, USA*, pages 17–18, 2010.

[16] Jiyu Zhang and Giorgio Rizzoni. Selection of residual generators in structural analysis for fault diagnosis using a diagnosability index. In *2017 IEEE Conference on Control Technology and Applications (CCTA)*, pages 1438–1445. IEEE, 2017.